

# FEASIBILITY OF HOM-FREE ACCELERATING RESONATORS: BASIC IDEAS AND IMPEDANCE CALCULATIONS

PAOLO ARCIONI

and

GIUSEPPE CONCIAURO

*Dipartimento di Elettronica dell'Università di Pavia,  
Via Abbiategrosso 209, I-27100 Pavia, Italy.*

*(Received 31 May 1991; in final form 11 September 1991)*

This paper is intended to demonstrate the feasibility of unconventional accelerating structures that fully suppress higher-order modes (HOMs). In these structures, unlike conventional cavities, the interaction region communicates through very large apertures with waveguides connected to absorbing terminations. The special geometry of the structure permits to trap in the interaction region a single high-Q resonating mode. For this reason these structures can be called 'Single Trapped Mode Resonators' (STMRs). After a discussion of the basic ideas underlying the operation of an STMR, an algorithm is presented that permits wideband calculation of the longitudinal and transverse beam-coupling impedances. Some numerical simulations are reported and compared with the experimental results from a model of an S-band STMR. Both numerical and experimental results show that, with careful dimensioning of the structure, very good HOM suppression is obtained, and that the shunt impedance and Q of the trapped mode are only slightly reduced compared to conventional accelerating cavities.

## 1. INTRODUCTION

The beam current circulating in synchrotrons operating with many bunches is limited by the longitudinal and transverse coupled-bunch instabilities. Bunch-to-bunch coupling is mediated by the electromagnetic oscillations generated by the beam in its environment, particularly via excitation of the higher-order modes (HOMs) of the accelerating cavities. The conditions for the instabilities are given in terms of the longitudinal and transverse beam coupling impedances,<sup>1</sup> whose frequency behavior is of paramount importance in this context. In particular these conditions show that instabilities are highly probable when the impedances exhibit crowds of sharp resonant peaks, like those determined by the HOMs of the accelerating cavities. Therefore the primary cure for preventing coupled-bunch instabilities consists of eliminating or smoothing these peaks without lowering the longitudinal impedance of the fundamental (accelerating) mode. The damping of HOMs is also a prerequisite for the cavities to be used in future TeV  $e^\pm$  linear colliders, where wakefield modes propagating in the periodic cavity chain must be heavily attenuated.

Many HOM dampers have been described in the recent literature, both for synchrotrons<sup>2, 3, 4, 5</sup> and for linear accelerators.<sup>6</sup> Most of them consist of absorbing loads connected to the cavity through waveguide sections whose cutoff frequency is between the frequency of the accelerating mode and the frequency of the first HOM. In this way the  $Q$  of the fundamental mode is substantially unaffected by the absorbers, whereas the  $Q$ s of the HOMs are lowered to different extents, depending on the coupling of these modes with the waveguides.

All dampers presented thus far have been conceived as extra devices added to a conventional cavity in such a way as to suppress a limited number of HOMs. Furthermore, in some cases, no definite strategy appears to underlie the number or positioning of the dampers or the design of the coupling region between the cavity body and the waveguides. For this reason the coupling of the HOMs to the absorbing loads is far from optimized, so it is not surprising that the experimental results show that a lot of HOMs resist the cure.

In a recent work<sup>7</sup> we suggested a strategy for realizing nonconventional resonators that are practically HOM-free. In designing these structures, which are more similar to symmetric waveguide junctions terminated by absorbing loads (Fig. 1) than to cavities with dampers, the absorbers are considered as a fundamental part rather than as a cure to be added afterwards, thus permitting optimized results. The central region of these structures, where the beam interaction takes place, communicates with the waveguides through very large apertures. If judiciously dimensioned, this region can trap a single high- $Q$  resonating mode (used for acceleration); yet, due to the strong coupling between the central region and the loads, no other high- $Q$  resonance above the frequency of this mode will be possible. As a result, the longitudinal and transverse beam-coupling impedances are small at any frequency, except for a single peak exhibited by the longitudinal impedance at the resonating frequency of the trapped mode. Due to the presence of a single high- $Q$  mode, these structures were named 'Single Trapped Mode Resonators' (STMRS).

The basic principles underlying the operation of STMRS are illustrated qualitatively in Section 2, which constitutes also an overview of our previous paper.<sup>7</sup> For simplicity, cylindrical or quasi-cylindrical structures are considered in this section. The definitions of the beam-coupling impedances for STMRS are presented in Section 3, and the theory for their calculation is developed in Sections 4–6. The specialization of this theory to the case of cylindrical structures is discussed in Section 7, where some numerical examples are reported together with other results for a quasi-cylindrical structure.

## 2. QUASI-CYLINDRICAL STMRS

First we consider the cylindrical structure shown in Fig. 2, consisting of a circular inner body connected through very large apertures to three rectangular waveguides, radially oriented and symmetrically placed around the  $z$  axis. This structure has threefold symmetry and exhibits three symmetry planes passing through the  $z$  axis.

At the beginning let us suppose that the waveguides are shorted at the ports  $S_1$ ,  $S_2$ , and  $S_3$  so that our structure becomes a cylindrical cavity having transverse cross section  $S$  (Fig. 2b) and height  $L$ . A beam traveling parallel to the  $z$  axis would excite only TM modes, which interact with it via the  $z$  component of the electric field. This component

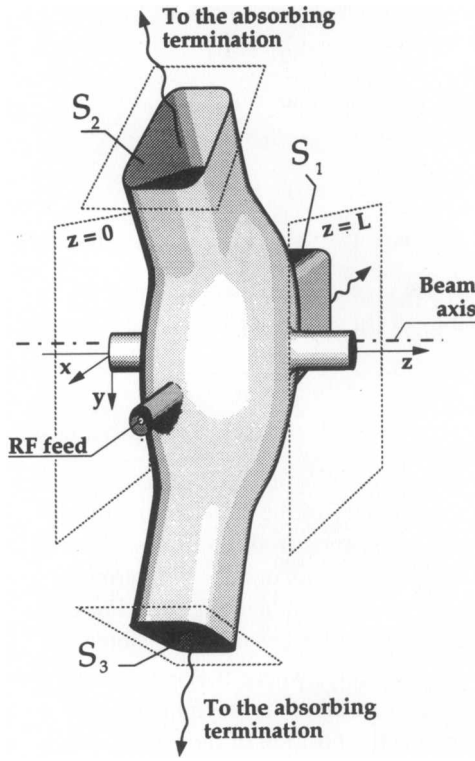


FIGURE 1 A possible STMR accelerating structure.

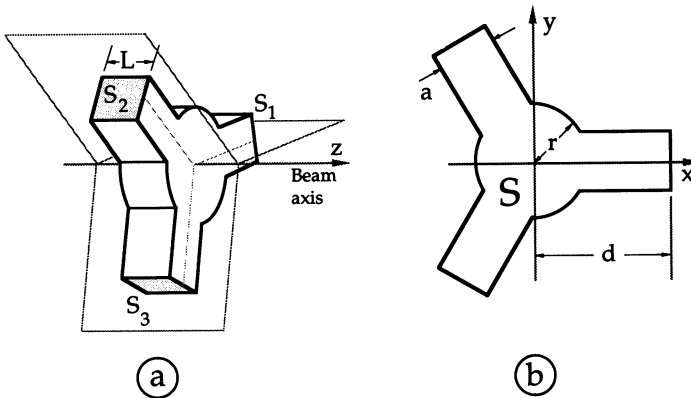


FIGURE 2 The cylindrical structure used for discussing the feasibility of an STMR.

has the product form

$$E_z = A\psi \cos(q\pi z/L) \quad (q = 0, 1, \dots) \quad (1)$$

where  $A$  is an arbitrary constant and  $\psi = \psi(x, y)$  is an eigenfunction of the two-dimensional eigenvalue problem

$$\begin{aligned} \nabla^2 \psi + \chi^2 \psi &= 0 \quad \text{in } S \\ \psi &= 0 \quad \text{over the boundary } C_s. \end{aligned}$$

It is well-known that the eigenvalues  $\chi$  are real and positive and that they determine the resonating frequencies of the modes. The resonant frequencies are given by

$$f = \frac{c}{2\pi} \sqrt{\chi^2 + (q\pi/L)^2} \quad (2)$$

where  $c$  is the speed of light.

Due to the complicated shape of  $S$ , the eigenfunctions and eigenvalues must be determined numerically. The symmetry of the structure permits to infer some particular properties of the modes, which are summarized as follows. With reference to the  $xz$  plane, the eigenfunctions can be classified as even or odd. Furthermore, some of them have the same threefold symmetry as the structure (others do not). For these reasons we can consider four groups of eigenfunctions and eigenvalues, denoted by  $\psi_p^{SE}, \psi_p^{AE}, \psi_p^{SO}, \psi_p^{AO}$  and  $\chi_p^{SE}, \chi_p^{SO}, \chi_p^{AE}, \chi_p^{AO}$  respectively, where the superscripts denote the symmetry ( $S \equiv$  rotationally symmetric,  $A \equiv$  rotationally asymmetric,  $E \equiv$  even,  $O \equiv$  odd) and the index  $p = 1, 2, \dots$  represents the position of the eigenvalue, assuming that in each group the eigenvalues are numbered in ascending order. Asymmetric eigenfunctions occur in degenerate pairs, i.e.,  $\chi_p^{AE} = \chi_p^{AO}$ . The four groups of eigenfunctions give rise to four classes of TM modes with the same symmetries, labeled with the symbols  $\text{TM}_{pq}^{SE}$ ,  $\text{TM}_{pq}^{SO}$ ,  $\text{TM}_{pq}^{AE}$ , and  $\text{TM}_{pq}^{AO}$ . All pairs of  $\text{TM}_{pq}^{AE}$  and  $\text{TM}_{pq}^{AO}$  with the same indices are degenerate.

The features of the mode patterns are better understood by considering Fig. 3, which shows the contour lines of some eigenfunctions calculated in the case  $r = 30$  mm,  $a = L = 35$  mm, and  $d = 73$  mm. The  $\psi_p^{SE}$  eigenfunctions have a maximum on the  $z$  axis, unlike all the other eigenfunctions, which are zero on the  $z$  axis. Therefore the only accelerating modes are those labeled with  $\text{TM}_{pq}^{SE}$ , since only these modes have a nonzero axial electric field on the  $z$  axis. Moreover, in asymmetric eigenfunctions  $\nabla\psi$  differs from zero at the  $z$  axis, so in the  $\text{TM}_{pq}^{AE}$  and  $\text{TM}_{pq}^{AO}$  modes the transverse gradient of  $E_z$  differs from zero there. This means that the action of asymmetric modes on the beam results in a transverse force<sup>8</sup> and that the  $\text{TM}_{pq}^{AE}$  and  $\text{TM}_{pq}^{AO}$  modes deflect the beam. Finally, the  $\psi_p^{SO}$  eigenfunctions have a saddle point at the  $z$  axis, so both  $\psi$  and  $\nabla\psi$  are zero there and  $\text{TM}_{pq}^{SO}$  modes do not interact with the beam, at least to the first order. The values of the resonating frequencies of the first modes associated with the eigenfunctions are also given in Fig. 3. Note that the fundamental mode is  $\text{TM}_{10}^{SE}$ , which, in the example considered, resonates in the S band (3.349 GHz).

Looking at the eigenfunctions of Fig. 3, we see that the eigenfunctions  $\psi_1^{SE}$  are evanescent inside the lateral waveguides, whereas all others are not. This result was obtained with a cut-and-try procedure involving the choice of the ratio  $a/r$ .

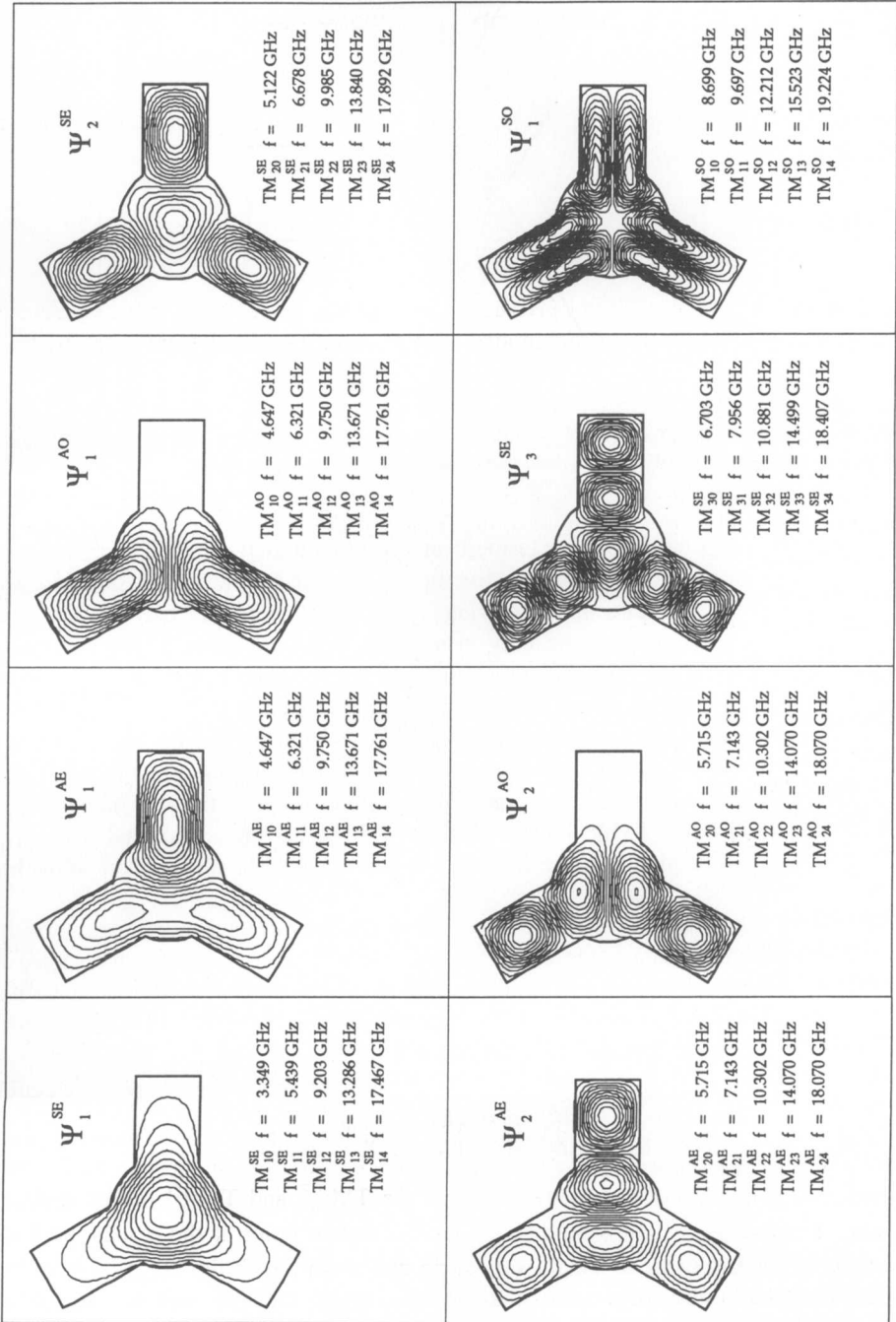


FIGURE 3 Numerically evaluated eigenfunctions and eigenvalues for the cross section of Fig. 2b, in the case  $r = 30$  mm,  $a = L = 35$  mm,  $d = 73$  mm. The contour lines of the eigenfunction are shown. The resonating frequencies of the first associated modes are also listed.

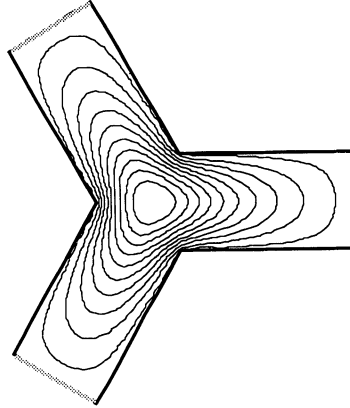


FIGURE 4 Contour lines for the  $\psi_1^{SE}$  eigenfunction in the limiting case  $a/r = \sqrt{3}$  (symmetric Y-junction). These lines correspond to the magnetic field mode pattern of the first trapped mode.

The modes depending on the evanescent eigenfunction (i.e., all  $\text{TM}_{1q}^{SE}$  are nearly confined in the central region of the structure. They can be viewed as standing waves generated by the total reflection occurring at the coupling region between the central body and the waveguides, where only evanescent fields are excited. By contrast, the modes depending on the other eigenfunctions are not confined in the central region and can be viewed as standing waves resulting from total reflection at the terminating shorts.

Now replace the shorts with matched loads. It is evident that the modes produced by the reflection from the shorts no longer exist, whereas all the  $\text{TM}_{1q}^{SE}$  modes that are evanescent in the waveguides are practically unaffected. The trapped mode with the lowest frequency is the  $\text{TM}_{10}^{SE}$  mode. This mode, if excited by an external rf generator, is suitable for acceleration because  $E_z$  is at a maximum and is  $z$ -independent at the beam axis.

The  $\psi_1^{SE}$  eigenfunction is still evanescent in the lateral waveguides when the ratio  $a/r$  reaches its maximum value of  $\sqrt{3}$  (symmetric Y-junction of waveguides; see Fig. 4). It is evident that as the  $a/r$  ratio is decreased, other eigenfunctions can be made evanescent, giving rise to other families of trapped modes. Numerical experiments reveal that the  $\text{TM}_{1q}^{SE}$  modes remain the only trapped modes down to  $a/r \approx 1$ . Below this value the asymmetric eigenfunctions  $\psi_1^{AE}, \psi_1^{AO}$  become evanescent in the waveguides, so all the deflecting modes  $\text{TM}_{1q}^{AE}$  and  $\text{TM}_{1q}^{AO}$  remain trapped too. Therefore, in the cylindrical structure we have considered thus far, the condition

$$1 < a/r < \sqrt{3} \quad (3)$$

must be fulfilled in order to suppress as many HOMs as possible.

The residual higher-order modes that remain trapped, together with the fundamental, should be suppressed in order to make an STMR. It is interesting to note that the resonant frequency of the fundamental mode is below the cutoff frequency of the waveguides (4.286 GHz in the example), whereas the resonating frequencies of all  $\text{TM}_{lq}^{SE}$  HOMs are larger. Thus the residual HOMs remain trapped in spite of the fact that their frequency is high enough for waveguide transmission. To understand this point, consider Fig. 5a,

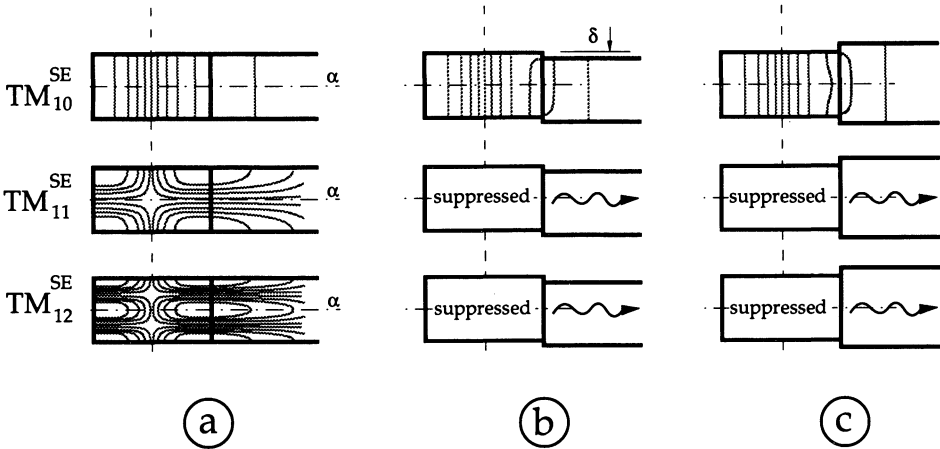


FIGURE 5 Electric field mode patterns in the  $xz$  plane for the first trapped modes in cylindrical (a) and quasi-cylindrical (b,c) structures. a) Due to the symmetry with respect to the  $\alpha$  plane, all  $TM_{1q}^{SE}$  modes are trapped. b) The offset  $\delta$  perturbs the symmetry and permits the excitation of the fundamental mode in the lateral waveguides. c) The waveguides with increased height permit the propagation of higher-order modes.

showing the E-field mode patterns in the  $xz$  plane. It is evident that, due to their  $z$ -dependence, modes other than  $TM_{10}^{SE}$  do not excite the fundamental  $TE_{10}$  mode of the waveguide, so no energy flow can take place through this mode. On the other hand, the waveguide modes excited by residual HOMs are below cutoff; for instance, the lowest guided modes excited by the  $TM_{11}^{SE}$  resonance are  $TE_{11}$  and  $TM_{11}$ , whose cutoff frequency (6.06 GHz) is higher than 5.432 GHz – that is, the resonant frequency of the  $TM_{11}^{SE}$  mode.

These considerations suggest two possible methods of suppressing residual HOMs: a) perturbing the symmetry with respect to the  $\alpha$  plane (see Fig. 5a), for instance, by offsetting the lateral waveguides in the  $z$ -direction, as shown in Fig. 5b; or b) increasing the height of the lateral waveguides (see Fig. 5c). Method a) permits the excitation of the fundamental mode in the waveguides; method b) can lower the cutoff frequency of the  $z$ -dependent guided modes below the resonating frequency of the exciting cavity mode. Both methods affect the resonant frequency of the fundamental  $TM_{10}^{SE}$  mode only slightly, since the perturbations are located in regions where its fields are quite small; therefore this mode remains trapped, its frequency lying below the cutoff frequency of the waveguide. In conclusion, cylindrical structures cannot achieve complete HOM suppression, whereas quasi-cylindrical structures, such as those resulting from methods a) or b), can become STMRs.

To demonstrate the feasibility of HOM suppression, measurements were carried out on an S-band experimental model having the same dimensions as the ones considered in the example of Fig. 3. Method a) was chosen to suppress residual HOMs; thus in the model the waveguides were displaced by a variable offset  $\delta$  in the  $z$  direction. The occurrence of the resonances of the accelerating modes was detected through observation of the transmission spectrum between two small probes lying on the  $z$  axis and placed on the opposite plane walls of the central body. The results are shown in Fig. 6, which

gives the transmitted power in dB, using as a reference the power transmitted at the resonant frequency of the fundamental mode. The spectrum in Fig. 6a was measured on the conventional cavity that was obtained by closing the central body by means of shorts at the planes where the waveguides would be inserted. This spectrum, considered for a better appreciation of the mode suppression, exhibits the familiar crowd of resonant peaks depending on the high-Q HOMs of the cavity. The spectrum in Fig. 6b was obtained after replacing the shorts by matched waveguides without any offset. This spectrum confirms the suppression of all accelerating modes except the  $TM_{1q}^{SE}$  family, whose survival is revealed by the peaks at 3.345, 5.432, 9.191, 13.265, and 17.443 GHz. (Note the closeness of these values to those calculated; see Fig. 3). Apart from these resonant peaks, the transmission spectrum is very broad as a result of the effective damping of all other accelerating modes. The spectrum of Fig. 6c was obtained after the introduction of an offset  $\delta = 5$  mm. It is noted that the transmission peak depending on the fundamental mode is practically unaffected, whereas the peaks related to the residual HOMs are typically lowered by 30 dB. Therefore, from a practical point of view, the only resonant mode which survives after the introduction of the offset is the fundamental.

Other transmission spectra were obtained after removing the probes and substituting a pair of small parallel loops in order to monitor the occurrence of deflecting HOMs. The results, not reported here, confirmed the suppression of all deflecting modes after the insertion of the matched waveguides, with or without offset.

The above considerations were based on a structure having a threefold symmetry axis, but, in principle, other symmetries could be considered. It is easy to see that a structure with a twofold axis should necessarily trap all deflecting modes with the symmetry shown in Fig. 7. On the other hand, structures having a fourfold or higher-order symmetry are not convenient, because they are more complicated and because the increased number of lateral waveguides decreases (or eliminates) the lateral clearance useful for rf power input. Therefore threefold symmetry appears to be the best choice.

### 3. DEFINITIONS OF THE EFFECTIVE VOLTAGES AND OF THE BEAM COUPLING IMPEDANCES

The coupling impedances describing the interaction between a beam and an accelerating structure are usually defined referring to axisymmetric resonant cavities (see Reference 8, for instance). This section aims at the generalization of these definitions to the case of an STMR structure having an  $N$ -fold rotational symmetry.

Let us consider the generic STMR structure shown in Fig. 1. The current density of a beam harmonic is represented by

$$\mathcal{J} = I_o f(x, y) e^{-jhz} \mathbf{u}_z \quad (e^{j\omega t} \text{ understood}) \quad (4)$$

where  $\mathbf{u}_z$  is the unit vector of the  $z$  axis;  $h$  is the wave number of the harmonic ( $h = \omega/\text{velocity of particles}$ );  $I_o$  is the current intensity of the harmonic at the  $z = 0$  plane; and  $f$  is a function of the transverse coordinates, describing the beam profile. Thus  $f$  differs from zero only near the  $z$  axis, in the small region crossed by the particles, and we have



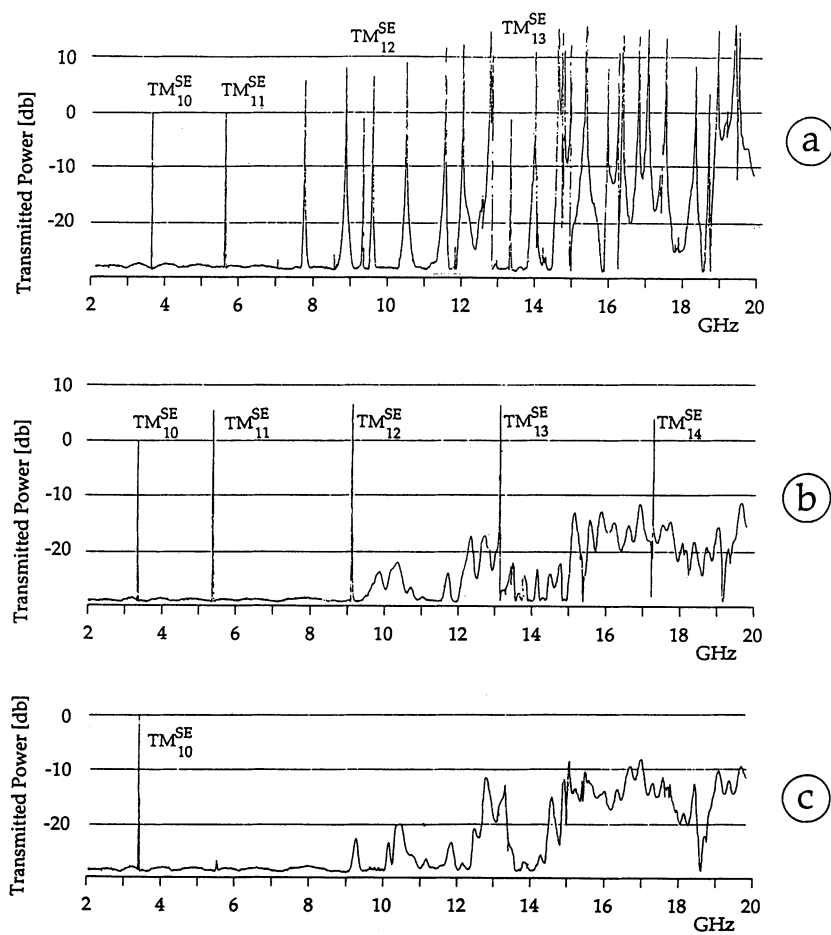


FIGURE 6 Measured transmission spectra of a model of STMR operating at *S*-band, having the dimensions  $r = 30$  mm,  $a = L = 35$  mm. The plots reports the transmitted power between two centered probes in the 2–20 GHz band; the reference is the transmitted power at the fundamental frequency. a) Waveguides shorted at a distance of 35 mm from the center. b) Matched waveguides, no offset. c) Matched waveguides, 5-mm offset.

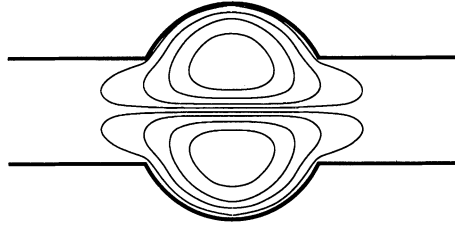


FIGURE 7 Magnetic field mode pattern of the first dipole mode trapped in a twofold-symmetric cavity connected to waveguides.

$$\int_{\sigma} f dx dy = 1 ; \quad \int_{\sigma} x f dx dy = \bar{x} ; \quad \int_{\sigma} y f dx dy = \bar{y} \quad (5)$$

where  $\sigma$  is the cross section of the beam pipe and  $\bar{x}, \bar{y}$  are the coordinates of the beam center. It is assumed that  $\bar{x}, \bar{y}$  are small with respect to the transverse dimension of the accelerating structure. Furthermore it is assumed that  $f$  is symmetric with respect to the beam center.

The beam harmonic at the frequency  $\omega$  generates in the accelerating structure a time-harmonic field at the same frequency. The electric and magnetic fields are represented by complex vectors  $\mathbf{E} = \mathbf{E}(x, y, z|\bar{x}, \bar{y})$ ,  $\mathbf{H} = \mathbf{H}(x, y, z|\bar{x}, \bar{y})$ . For a given structure and a given beam profile, the field depends on the position of the beam center. Moreover, it is assumed that the field amplitude in the beam region is significant only in the interval  $0 < z < L$  including the STMR structure (see Fig. 1).

The energy and the momentum gained by a unit point charge crossing the accelerating structure result from the contribution due to the interaction of the charge with all the harmonics. Consider a point charge moving parallel to the  $z$  axis at the coordinates  $x, y$  and crossing the  $z = 0$  plane at the time  $t_o$ . The energy gained at the frequency  $\omega$  is given by  $Re(v_{\parallel} \exp(j\omega t_o))$ , where  $v_{\parallel}$  is the 'effective accelerating voltage' defined as<sup>8</sup>

$$v_{\parallel} = v_{\parallel}(x, y|\bar{x}, \bar{y}) = \int_0^L E_z(x, y, z|\bar{x}, \bar{y}) e^{jh_z z} dz.$$

The transverse momentum gained by the same charge is given by  $Re\{v_{\perp} \exp(j\omega t_o)\}$ , where the vector  $v_{\perp}$  is the 'effective deflecting voltage' defined as<sup>8</sup>:

$$v_{\perp} = v_{\perp}(x, y|\bar{x}, \bar{y}) = -\frac{c}{j\omega} \int_0^L \nabla_{\perp} E_z(x, y, z|\bar{x}, \bar{y}) e^{jh_z z} dz,$$

where  $\nabla_{\perp} = \mathbf{u}_x \partial_x + \mathbf{u}_y \partial_y$ .

The average values of the accelerating and deflecting voltages in the bunch are given by

$$V_{\parallel} = V_{\parallel}(\bar{x}, \bar{y}) = \int_{\sigma} f v_{\parallel} dx dy = \int_{\sigma} \int_0^L f E_z(x, y, z|\bar{x}, \bar{y}) e^{jh_z z} dx dy dz \quad (6a)$$

$$\begin{aligned} V_{\perp} &= V_{\perp}(\bar{x}, \bar{y}) = \int_{\sigma} f v_{\perp} dx dy \\ &= -\frac{c}{j\omega} \int_{\sigma} \int_0^L f \nabla_{\perp} E_z(x, y, z | \bar{x}, \bar{y}) e^{jh z} dx dy dz \quad . \end{aligned} \quad (6b)$$

Note that, due to the linearity of the field equations,  $E_z$ ,  $V_{\parallel}$  and  $V_{\perp}$  are proportional to  $I_o$ . Since we consider small values of  $\bar{x}, \bar{y}$ , in the evaluation of  $V_{\parallel}$  it is possible to assume that the beam is centered. With this assumption  $V_{\parallel}$  is related to  $I_o$  by the ‘longitudinal beam coupling impedance’, defined by

$$Z_{\parallel}[\Omega] = -\frac{V_{\parallel}(0, 0)}{I_o} = -\frac{1}{I_o} \int_{\sigma} \int_0^L f E_z(x, y, z | 0, 0) e^{jh z} dx dy dz \quad . \quad (7)$$

The symmetry of the structure and of the beam profile permits us to infer that, in the case  $\bar{x} = \bar{y} = 0$ ,  $E_z$  must have a maximum on the  $z$  axis, i.e., that  $\nabla_{\perp} E_z = 0$ . Therefore no deflecting voltage exists in the case of a centered beam. In fact a deflecting voltage can arise only if the beam crosses the accelerating structure off-axis. Provided  $x$  and  $\bar{y}$  are small, the components of the deflecting voltage must be linear combinations of the coordinates of the beam center, and we can write:

$$V_x = -j I_o (Z_{xx} \bar{x} + Z_{xy} \bar{y})$$

$$V_y = -j I_o (Z_{yx} \bar{x} + Z_{yy} \bar{y}) \quad ,$$

where the coefficients  $Z_{\alpha\beta}$ , which depend on the accelerating structure, are the components of the tensor relating the deflecting voltage to the beam displacement. This tensor represents in general the transverse coupling impedance of the accelerating structure.

In an  $N$ -fold symmetric structure the tensor  $Z_{\alpha\beta}$  must be invariant with respect to a rotation of the  $x$  and  $y$  axes by an angle of  $2\pi/N$ . It is easily verified that for  $N \geq 3$  this implies  $Z_{xx} = Z_{yy}$  and  $Z_{xy} = -Z_{yx}$ . Moreover, if the accelerating structure has a reflection symmetry with respect to the  $xz$  plane (see Fig. 1), a beam displaced in the  $x$  direction ( $\bar{y} = 0$ ) generates a deflecting voltage in the same direction ( $V_y = 0$ ). Therefore we have  $Z_{yx} = 0$  and, consequently,  $Z_{xy} = 0$ . In conclusion, if we define  $Z_{xx} = Z_{yy} = Z_{\perp}$ , the symmetry of the structure implies that  $V_x = Z_{\perp} \bar{x}$  and  $V_y = Z_{\perp} \bar{y}$ , so the transverse impedance becomes a scalar quantity and we can write

$$V_{\perp} = -j Z_{\perp} I_o (\bar{x} \mathbf{u}_x + \bar{y} \mathbf{u}_y) \quad . \quad (8)$$

This expression shows that  $Z_{\perp}$  can be calculated assuming a beam deflected in the  $x$ -direction. Thus we have

$$Z_{\perp}[\Omega/m] = j \frac{V_x}{I_o \bar{x}} = -\frac{c}{\omega I_o \bar{x}} \int_{\sigma} \int_0^L f \partial_x E_z(x, 0, z | \bar{x}, 0) e^{jh z} dx dy dz \quad . \quad (9)$$

Note that Eqs. (7-9) coincide with the standard definitions of the beam coupling impedances for axisymmetric cavities. However, Eqs. (8) and (9) hold only for structures having a threefold (or higher-order) rotational symmetry, plus the symmetry planes.

## 4. EVALUATION OF THE FIELD GENERATED BY THE BEAM

The longitudinal and transverse coupled bunch instabilities depend on the frequency behavior of  $\text{Re}\{Z_{\parallel}\}$  and  $\text{Re}\{Z_{\perp}\}$  respectively, in the frequency range where the beam harmonics are significant (roughly speaking, the maximum frequency of interest is of the order of the velocity of the particles divided by the bunch length). In turn, the calculation of  $Z_{\parallel}$  and  $Z_{\perp}$  requires the determination of  $E_z$  in this frequency range.

The field will be studied in the volume  $V$  bounded by the conducting walls, by the ports  $S_1, S_2, S_3$  and by the transverse sections of the beam pipe placed at  $z = 0$  and  $z = L$  (see Fig. 1). Since the field is negligible in these sections, in the field calculation it is possible to assume that the beam pipe is closed by electric walls there. Obviously, this assumption is acceptable only at frequencies that are lower than the cutoff frequency of the beam pipe. Therefore the following analysis is meaningful only up to this frequency.

The field in the region  $V$  is determined by the current density  $\mathcal{J}$  and by the tangential electric field at the ports. According to waveguide theory, the transverse fields at the  $m$ th port ( $m = 1, 2, 3$ ) are given by:

$$\mathbf{E}_T^{(m)} = \sum_1^P V_p^{(m)} \mathbf{e}_p \quad (10a)$$

$$\mathbf{H}_T^{(m)} = \sum_1^P I_p^{(m)} \mathbf{h}_p \quad (10b)$$

where  $\mathbf{e}_p, \mathbf{h}_p$  denote the electric and magnetic modal vector of the  $p$ th mode and  $I_p^{(m)}, V_p^{(m)}$  represent the current and the voltage for this mode evaluated at the  $m$ th port. We recall that:

$$\int_{S_m} \mathbf{h}_p \cdot \mathbf{h}_q dS_m = \int_{S_m} \mathbf{e}_p \cdot \mathbf{e}_q dS_m = \delta_{pq} \quad (11a)$$

$$\mathbf{n} \times \mathbf{e}_p = \mathbf{h}_p \quad (11b)$$

where  $\mathbf{n}$  is the outward unit vector normal to the port and  $\delta_{pq}$  is Kroneker's symbol. In Eq. (10), both the TE and the TM modes are involved; they are labeled using a single index, and are numbered according to the non-decreasing order of their cutoff frequencies. Though the summations should consist of an infinite number of terms, only the first  $P$  terms are retained, corresponding to the modes which propagate or are only a little below cutoff at the maximum frequency of interest. In fact, these are the only modes that have a significant amplitude, assuming that the ports are placed far enough from the central body. From Eqs. (10) and (11) we have:

$$I_p^{(m)} = \int_{S_m} \mathbf{H}_T^{(m)} \cdot \mathbf{h}_p dS_m \quad (12a)$$

$$V_p^{(m)} = \int_{S_m} (\mathbf{n} \times \mathbf{E}_T^{(m)}) \cdot \mathbf{h}_p dS_m \quad (12b)$$

Due to the absorbing terminations connected to the waveguides, the modal currents and voltages must be related by

$$I_p^{(m)} = Y_p V_p^{(m)} \quad (m = 1, 2, 3; p = 1, \dots, P) \quad (13)$$

where  $Y_p$  is the admittance of the termination for the  $p$ th mode. Equations (10–13) together permit us to relate  $\mathbf{E}_T^{(m)}$  and  $\mathbf{H}_T^{(m)}$ ; for this reason they represent the boundary condition imposed at the ports.

Assuming perfectly conducting walls, the field in the bounded region  $V$  can be expanded into irrotational and solenoidal eigenvectors, according to the ‘theory of cavity resonators’ (see Ref. 9, for instance). Taking into account Eqs. (10) and (11), we have:

$$\begin{aligned} \mathbf{E} = & -I_o \frac{c}{j\omega} \sum_i F_i \mathbf{f}_i - jI_o \omega \eta c \sum_i \frac{D_i}{\omega_i^2 - \omega^2} \boldsymbol{\mathcal{E}}_i + \\ & -c \sum_i \frac{\omega_i}{\omega_i^2 - \omega^2} \boldsymbol{\mathcal{E}}_i \sum_1^3 m \sum_1^P p V_p^{(m)} C_{ip}^{(m)} \end{aligned} \quad (14a)$$

$$\begin{aligned} \mathbf{H} = & c I_o \sum_i \frac{\omega_i D_i}{\omega_i^2 - \omega^2} \boldsymbol{\mathcal{H}}_i - \frac{c}{j\omega \eta} \sum_i \mathbf{g}_i \sum_1^3 m \sum_1^P p V_p^{(m)} G_{ip}^{(m)} + \\ & -\frac{j\omega c}{\eta} \sum_i \frac{\boldsymbol{\mathcal{H}}_i}{\omega_i^2 - \omega^2} \sum_1^3 m \sum_1^P p V_p^{(m)} C_{ip}^{(m)} \end{aligned} \quad (14b)$$

where  $\eta = 377\Omega$  is the characteristic impedance of vacuum;  $\mathbf{f}_i$  and  $\mathbf{g}_i$  are the electric and magnetic irrotational eigenvectors;  $\boldsymbol{\mathcal{E}}_i$  and  $\boldsymbol{\mathcal{H}}_i$  are the electric and the magnetic divergenceless eigenvectors corresponding to the electric and magnetic fields of the resonant modes of the cavity obtained when the ports are shorted; and  $\omega_i$  represent the resonant frequencies of these modes. Moreover,

$$D_i = \int_{\sigma} \int_0^L \mathbf{u}_z \cdot \boldsymbol{\mathcal{E}}_i f e^{-jhz} dx dy dz \quad (14c)$$

$$F_i = \int_{\sigma} \int_0^L \mathbf{u}_z \cdot \mathbf{f}_i f e^{-jhz} dx dy dz \quad (14d)$$

$$C_{ip}^{(m)} = \int_{S_m} \boldsymbol{\mathcal{H}}_i \cdot \mathbf{h}_p dS_m \quad (14e)$$

$$G_{ip}^{(m)} = \int_{S_m} \mathbf{g}_i \cdot \mathbf{h}_p dS_m \quad (14f)$$

The eigenvectors are normalized according to

$$\int_V \mathbf{f}_i \cdot \mathbf{f}_i dV = 1 ; \quad \int_V \mathbf{g}_i \cdot \mathbf{g}_i dV = 1 ; \quad \int_V \boldsymbol{\mathcal{E}}_i \cdot \boldsymbol{\mathcal{E}}_i dV = 1 ; \quad \int_V \boldsymbol{\mathcal{H}}_i \cdot \boldsymbol{\mathcal{H}}_i dV = 1 .$$

It is assumed that the resonant modes are numbered in the non-decreasing order of their frequencies.

In principle, by using Eq. (14b) to represent the magnetic field at the ports and substituting into Eq. (12a),  $I_p^{(m)}$  can be expressed in terms of  $I_o$  and  $V_p^{(m)}$ . The

boundary conditions of Eq. (13) can be used to eliminate  $I_p^{(m)}$ , thus obtaining a system which yields the modal voltages as functions of the beam current. Once all voltages  $V_p^{(m)}$  are known, Eq. (14a) permits evaluation of the electric field in the beam region. Unfortunately, the slow convergence of the series involving the index  $i$  in Eqs. (14a,b) makes this approach almost unfeasible, since it would require the numeric evaluation of a large number of irrotational and divergenceless eigenvectors. This drawback can be overcome because, in representing the electric field on the axis and the magnetic field at the ports (which are the only fields involved in the calculation), it is possible to accelerate the convergence of the series as described below. Following the Kummer procedure,<sup>10</sup> we write:

$$\begin{aligned} \mathbf{E} = & \mathbf{E}_{qs} - jI_o\eta c\omega^3 \sum_i \frac{D_i}{\omega_i^2(\omega_i^2 - \omega^2)} \boldsymbol{\mathcal{E}}_i + \\ & -c\omega^2 \sum_i \frac{\boldsymbol{\mathcal{E}}_i}{\omega_i(\omega_i^2 - \omega^2)} \sum_1^3 m \sum_1^P p V_p^{(m)} C_{ip}^{(m)} \end{aligned} \quad (15a)$$

$$\begin{aligned} \mathbf{H} = & \mathbf{H}_{qs} + I_o c\omega^2 \sum_i \frac{D_i}{\omega_i(\omega_i^2 - \omega^2)} \boldsymbol{\mathcal{H}}_i + \\ & -\frac{j c\omega^3}{\eta} \sum_i \frac{\boldsymbol{\mathcal{H}}_i}{\omega_i^2(\omega_i^2 - \omega^2)} \sum_1^3 m \sum_1^P p V_p^{(m)} C_{ip}^{(m)} \end{aligned} \quad (15b)$$

where the extracted fields  $\mathbf{E}_{qs}$  and  $\mathbf{H}_{qs}$  are:

$$\begin{aligned} \mathbf{E}_{qs} = & -I_o \frac{c\eta}{j\omega} \sum_i F_i \mathbf{f}_i - jI_o\omega\eta c \sum_i \frac{\boldsymbol{\mathcal{E}}_i D_i}{\omega_i^2} + \\ & -c \sum_i \frac{\boldsymbol{\mathcal{E}}_i}{\omega_i} \sum_1^3 m \sum_1^P p V_p^{(m)} C_{ip}^{(m)} \end{aligned} \quad (16a)$$

$$\begin{aligned} \mathbf{H}_{qs} = & cI_o \sum_i \frac{D_i}{\omega_i} \boldsymbol{\mathcal{H}}_i - \frac{c}{j\omega\eta} \sum_i \mathbf{g}_i \sum_1^3 m \sum_1^P p V_p^{(m)} G_{ip}^{(m)} + \\ & -\frac{j\omega c}{\eta} \sum_i \frac{\boldsymbol{\mathcal{H}}_i}{\omega_i^2} \sum_1^3 m \sum_1^P p V_p^{(m)} C_{ip}^{(m)} \end{aligned} \quad (16b)$$

After the extraction of the partial fields  $\mathbf{E}_{qs}$  and  $\mathbf{H}_{qs}$ , the series appearing in Eq. (15) converge much more rapidly than the original ones, because their terms go to zero as fast as  $\omega_i^{-3}$  or  $\omega_i^{-4}$ . This feature, of course, can be exploited only if the partial fields can be determined independently of the series in Eq. (16). Note that, for given values of  $I_o$ ,  $h$ , and  $V_p^{(m)}$  and when  $\omega \rightarrow 0$ , we have  $\mathbf{E} \rightarrow \mathbf{E}_{qs}$ ,  $\mathbf{H} \rightarrow \mathbf{H}_{qs}$ . Thus  $\mathbf{E}_{qs}$  and  $\mathbf{H}_{qs}$  can be viewed as the quasi-static fields that would be excited inside the STMR if the current density  $\mathcal{J}$  and the modal voltages  $V_p^{(m)}$  were acting at low frequency.

Since  $\mathbf{H}_{qs}$  must be determined at the ports only, Eq. (16b) can be transformed into a more useful one. In fact, a low-frequency excitation produces evanescent fields into the

lateral waveguides. Therefore, in the evaluation of  $\mathbf{H}_{qs}$  at the  $m$ th port, it is possible to neglect the effect of both the beam current and the modal voltages at the other ports. Thus we have

$$\mathbf{H}_{qs}^{(m)} \approx - \sum_1^P V_p^{(m)} \left( \frac{c}{j\omega\eta} \sum_i \mathbf{g}_i G_{ip}^{(m)} + \frac{j\omega c}{\eta} \sum_i \frac{\mathbf{H}_i}{\omega_i^2} C_{ip}^{(m)} \right) . \quad (17)$$

According to Eq. (17), the only sources of  $\mathbf{H}_{ip}^{(m)}$  are the modal voltages  $V_p^{(m)}$ . On the other hand, for any guided mode the current produced by  $V_p^{(m)}$  towards the *inside* of the structure (i.e.,  $-I_p^{(m)}$ ) at low frequency is given by

$$-I_p^{(m)} = j B_p V_p^{(m)} ,$$

where  $jB_p$  represents the characteristic impedance of the  $p$ th mode, which is reactive below cutoff. This relation can be written because the low-frequency field produced into the structure is evanescent and consequently the length of the lateral waveguide sections can be considered infinite. Therefore we can write:

$$\mathbf{H}_{ip}^{(m)} \approx -j \sum_1^P V_p^{(m)} B_p \mathbf{h}_p . \quad (18)$$

Comparing Eqs. (17) and (18), we see that the term in brackets in the former equation represents  $jB_p \mathbf{h}_p$  or, more specifically, its power expansion with respect to  $\omega$ , truncated up to the first order. Considering the power expansion of the well-known expressions of the characteristic impedance of the TE and TM modes, we find that:

$$jB_p \approx \begin{cases} \frac{1}{\eta} \left( \frac{\omega_{cp}}{j\omega} + \frac{j\omega}{2\omega_{cp}} \right) & \text{(if the } p^{\text{th}} \text{ mode is a TE mode)} \quad (19a) \\ j \frac{\omega}{\eta\omega_{cp}} & \text{(if the } p^{\text{th}} \text{ mode is a TM mode)} \quad (19b) \end{cases}$$

where  $\omega_{cp}$  denotes the cutoff frequency of the  $p$ th mode. In conclusion, when evaluating Eq. (15b) at the  $m$ th port,  $\mathbf{H}_{qs}$  can be represented in closed form by Eq. (18).

Following a similar argument, it is possible to simplify Eq. (16a). In fact, when calculating  $\mathbf{E}_{qs}$  near the axis, it is possible to neglect the contribution of the modal voltages  $V_p^{(m)}$  because, due to the cutoff properties of the waveguides, at low frequency the ports are substantially decoupled from the central body. Therefore it is possible to write:

$$\mathbf{E}_{qs} \approx - \left( \frac{c\eta}{j\omega} \sum_i F_i \mathbf{f}_i + j I_o \omega \eta c \sum_i \frac{\boldsymbol{\varepsilon}_i D_i}{\omega_i^2} \right) I_o . \quad (20)$$

As will become apparent below, with this approximation  $\mathbf{E}_{qs}$  contributes to the coupling impedances only through a non-resonant reactive term, not relevant to stability. For this reason transforming Eq. (20) into a more rapidly converging one deserves no

attention. Substituting Eq. (15b) into Eq. (12a), taking into account Eqs. (11a) and (13), we obtain the following system:

$$\begin{aligned} (Y_p + jB_p)Z_p^{(m)} + j\frac{c\omega^3}{\eta} \sum_1^3 n \sum_1^P q \sum_i \frac{C_{ip}^{(n)} C_{iq}^{(n)}}{\omega_i^2 (\omega_i^2 - \omega^2)} Z_q^{(n)} = \\ = c\omega^2 \sum_i \frac{C_{ip}^{(m)} D_i}{\omega_i (\omega_i^2 - \omega^2)} \quad (m = 1, 2, 3; p = 1, 2, \dots, P) \end{aligned} \quad (21)$$

where the quantities

$$Z_p^{(m)} = V_p^{(m)} / I_o \quad (22)$$

represent the transimpedances between  $I_o$  and the mode voltages. Equation (21) yields the  $3 \times P$  transimpedances, which permit us to express the variables  $V_p^{(m)}$  as functions of  $I_o$ . Therefore, on substitution into Eq. (15a), we are able to express the electric field as a function of the beam current only.

## 5. CALCULATION OF THE LONGITUDINAL BEAM COUPLING IMPEDANCE

Substituting Eq. (15a) into Eq. (7), and taking into account the transimpedances of Eq. (22), we have:

$$\begin{aligned} Z_{\parallel} = jX_{qs_{\parallel}} + j\eta c\omega^3 \sum_1^M i \frac{|D_i|^2}{\omega_i^2 (\omega_i^2 - \omega^2)} + \\ c\omega^2 \sum_1^M i \frac{D_i^*}{\omega_i (\omega_i^2 - \omega^2)} \sum_i^3 m \sum_1^P p C_{ip}^{(m)} Z_p^{(m)} \end{aligned} \quad (23a)$$

where the star denotes the conjugate and, moreover,

$$X_{qs_{\parallel}} = \frac{j}{I_o} \int_{\sigma} \int_0^L \mathbf{u}_z \cdot \mathbf{E}_{qs} f e^{jhz} dx dy dz = -\frac{\eta c}{\omega} \sum_i |F_i|^2 + \omega \eta c \sum_i \frac{|D_i|^2}{\omega_i^2} \quad (23b)$$

Note that  $X_{qs_{\parallel}}$  is a real quantity, so its contribution to the impedance is purely reactive. Moreover, the series in Eq. (23a) were truncated, retaining only the first  $M$  terms. This was possible due to the rapid convergence of the series: as a rule of thumb, retaining the modes having resonant frequencies below 1.5 times the maximum frequency of interest is sufficient for achieving good accuracy.

Let us consider the coefficients  $D_i$ , which depend on the  $z$ -component of the eigenvectors of the first  $M$  modes. From now on, this component will be denoted by  $E_i$ . It is possible to assume that, in the beam region, the transverse variation of  $E_i$  is slow enough to permit the approximation

$$E_i \approx (E_i)_o + x(\partial_x E_i)_o + y(\partial_y E_i)_o \quad (24)$$



where the subscript 'o' denotes quantities evaluated at  $x = y = 0$ . Using this approximation, and taking into account Eq. (5), it is easily shown that:

$$\int_{\sigma} \int_0^L \mathbf{E}_i f e^{jh_z} dx dy dz \approx \int_0^L (\mathbf{E}_i)_o e^{jh_z} dz + \bar{x} \int_0^L (\partial_x \mathbf{E}_i)_o e^{jh_x} dz + \bar{y} \int_0^L (\partial_y \mathbf{E}_i)_o e^{jh_y} dz \quad . \quad (25)$$

According to Eq. (7), when evaluating  $Z_{\parallel}$  we assume a centered beam ( $\bar{x} = \bar{y} = 0$ ). Thus we have

$$D_i = \int_0^L (\mathbf{E}_i)_o e^{jh_z} dz \quad . \quad (26)$$

The considerations of in Section 2 regarding the classification and the general properties of the modes inside a threefold-symmetric structure hold in the case of a three-dimensional structure as well. Thus, recalling that the only modes having  $(\mathbf{E}_i)_o \neq 0$  are the SE modes, we see that  $D_i$  is zero except in these modes. Therefore only the SE modes are important in the determination of  $Z_{\parallel}$ .

Until now the effect of wall losses has been neglected. It can be taken into account using the same approximation made in the study of forced oscillations of cavity resonators. This approximation consists in making everywhere the following substitution:

$$\frac{1}{\omega_i^2 - \omega^2} \rightarrow \frac{1}{\omega_i^2 + j \frac{\omega \omega_i}{Q_i} - \omega^2} \quad , \quad (27)$$

where  $Q_i$  is the quality factor of the  $i$ th resonance.

In conclusion, the scheme for the calculation of  $Re\{Z_{\parallel}\}$  is:

- a) Determine the first  $M$  eigenvectors  $\mathcal{E}_i, \mathcal{H}_i$  and the corresponding frequencies and  $Q$  factors.
- b) Evaluate the coefficients  $C_{ip}^{(m)}$  using Eq. (14e), where the waveguide mode vectors are assumed to be known.

Moreover, for any frequency  $\omega$ :

- c) Evaluate the coefficients  $D_i$  using Eq. (26).
- d) Determine the transimpedances  $Z_p^{(m)}$  solving the system:

$$\begin{aligned} (Y_p + jB_p)Z_p^{(m)} + j \frac{c\omega^3}{\eta} \sum_1^3 n \sum_1^P q \sum_1^M i \frac{C_{ip}^{(n)} C_{iq}^{(n)}}{\omega_i^2 (\omega_i^2 + j\omega\omega_i/Q_i - \omega^2)} Z_q^{(n)} = \\ = c\omega^2 \sum_1^M i \frac{C_{ip}^{(m)} D_i}{\omega_i (\omega_i^2 + j\omega\omega_i/Q_i - \omega^2)} \cdot (m = 1, 2, 3; p = 1, 2, \dots, P) \quad (28) \end{aligned}$$

e) Calculate:

$$\begin{aligned} \operatorname{Re}\{Z_{\parallel}\} &= \operatorname{Re}\left\{j\eta c\omega^3 \sum_1^M i \frac{|D_i|^2}{\omega_i^2(\omega_i^2 + j\omega\omega_i/Q_i - \omega^2)}\right\} + \\ &+ c\omega^2 \operatorname{Re}\left\{\sum_1^M i \frac{D_i^*}{\omega_i(\omega_i^2 + j\omega\omega_i/Q_i - \omega^2)} \sum_1^3 m \sum_1^P p C_{ip}^{(m)} Z_p^{(m)}\right\} \quad (29) \end{aligned}$$

If desired, only the SE modes can be considered in these calculations. The symmetry of these modes permits some simplifications<sup>11</sup> because all quantities become independent of the index  $m$ . It is noted, however, that the numerical selection of SE modes may overwhelm the advantage of exploiting the symmetry.

## 6. CALCULATION OF THE TRANSVERSE BEAM COUPLING IMPEDANCE

Introducing Eq. (15a) into Eq. (9), we obtain an expression containing the integrals

$$\int_{\sigma} \int_0^L f \partial_x \mathbf{E}_i e^{jhz} dx dy dz \quad .$$

From Eqs. (24) and (5), we obtain

$$\int_{\sigma} \int_0^L f \partial_x \mathbf{E}_i e^{jhz} dx dy dz = \int_0^L (\partial_x \mathbf{E}_i)_0 e^{jhz} dz \quad . \quad (30)$$

These integrals differ from zero only for AE modes, which are the only modes having  $\partial_x \mathbf{E}_i \neq 0$  at the axis. Thus only these modes are important in the evaluation of  $Z_{\perp}$ . Since the electric field at the  $z$ -axis is zero for these modes according to Eq. (25), and recalling that in this calculation we set  $\bar{y} = 0$ , we have:

$$D_i = \int_{\sigma} \int_0^L f \mathbf{E}_i^{AE} e^{-jhz} dx dy dz \approx \bar{x} \int_0^L (\partial_x \mathbf{E}_i^{AE})_0 e^{-jhz} dz = \bar{x} d_i \quad , \quad (31a)$$

where

$$d_i = \int_0^L (\partial_x \mathbf{E}_i^{AE})_0 e^{-jhz} dz \quad . \quad (31b)$$

Since  $(\partial_x \mathbf{E}_i)_0$  differs from zero only for AE modes, the selection of these modes in the calculation of  $Z_{\perp}$  may be avoided. In fact, for all modes other than AE ones, Eq. (31b) gives  $d_i = 0$ . For this reason, the superscript AE will be dropped hereafter.

Equation (31a) implies that the unknowns  $Z_p^{(m)}$  obtained from Eq. (21) are proportional to  $\bar{x}$ . Therefore it is convenient to replace the variables  $Z_p^{(m)}$  with these new ones:

$$z_p^{(m)} = Z_p^{(m)} / \bar{x} \quad (32)$$

so that Eq. (21) becomes:

$$\begin{aligned}
 (Y_p + jB_p)z_p^{(m)} + j\frac{c\omega^3}{\eta} \sum_1^3 n \sum_1^P q \sum_1^M i \frac{C_{ip}^{(n)} C_{iq}^{(n)}}{\omega_i^2(\omega_i^2 + j\omega\omega_i/Q_i - \omega^2)} z_q^{(n)} = \\
 = c\omega^2 \sum_1^M i \frac{C_{ip}^{(m)} d_i}{\omega_i(\omega_i^2 + j\omega\omega_i/Q_i - \omega^2)} \quad (m = 1, 2, 3, p = 1, 2, \dots, P) \quad (33)
 \end{aligned}$$

Taking into account Eqs. (9), (15a), (31a,b) and (32), we have:

$$\begin{aligned}
 Re\{Z_\perp\} = Re \left\{ j\eta c^2 \omega^2 \sum_1^M i \frac{|d_i|^2}{\omega_i^2(\omega_i^2 + j\omega\omega_i/Q_i - \omega^2)} \right\} + \\
 + c^2 \omega Re \left\{ \sum_1^M i \frac{d_i^*}{\omega_i(\omega_i^2 + j\omega\omega_i/Q_i - \omega^2)} \sum_1^3 m \sum_1^P p C_{ip}^{(m)} z_p^{(m)} \right\} \quad (34)
 \end{aligned}$$

Note also that, in evaluation of the real part of the transverse impedance, the contribution of the quasi-static field does not appear, because it results into a reactive term.

In conclusion, the scheme for the calculation of  $Re\{Z_\perp\}$  differs from that described in the previous section only in steps c), d), and e). These are modified as follows:

- c) Evaluate the coefficients  $d_i$  using Eq. (31b).
- d) Determine the quantities  $z_p^{(m)}$  solving Eq. (33).
- e) Calculate  $Re\{Z_\perp\}$  using Eq. (34).

## 7. NUMERICAL EXPERIMENTS

The described algorithm was used to determine the beam coupling impedances of the cylindrical structure considered in Fig. 2. In this case only the TM-*to-z* resonant modes are relevant in the calculation; more specifically, only the  $TM_{pq}^{SE}$  and  $TM_{pq}^{AE}$  modes are important. Their frequencies,  $Q$ -factors, and fields depend on the eigenvalues  $\chi$  and on the eigenfunctions  $\psi$  defined in Section 2, according to the expressions given in Table 1 (where the superscript  $X$  stands for  $S$  or  $A$ ). The quantity  $E_{pq}^{XE}$  represents the  $z$  component of the electric-mode vector, which is the only component involved in the calculations. The quantity  $R_s$  is the surface resistance of the conducting walls. The eigenfunctions  $\psi$ 's are normalized as shown in the table. The same table reports the functions  $h_{mn}^{TE}$  and  $h_{mn}^{TM}$ , which represent the transverse-to- $z$  component of the magnetic-mode vectors for the TE and TM modes of the rectangular waveguide. In fact, only this component is involved in Eq. (14e), since  $\mathcal{H}_{pq}^{XE}$  is transverse to  $z$ . Functions  $h_{mn}^{TE}$  and  $h_{mn}^{TM}$  are given with reference to the local coordinate  $\xi$  (see inset in the table). In the calculations, eigenfunctions  $\psi$  and eigenvalues  $\chi$  were obtained using an efficient two-dimensional electromagnetic solver (PAGODA).<sup>12</sup>

The results of the first numerical experiment are reported in the plots of Figs. 8 and 9. They show the real part of the longitudinal and transverse impedances, in the frequency band extending up to 15 GHz, which is about 4.5 times the fundamental resonant frequency (3.35 GHz).  $Re\{Z_\parallel\}$  is normalized to the shunt impedance  $R_\parallel$  of

$$\omega_{pq}^{XE} = c \sqrt{(\chi_p^{XE})^2 + (q\pi/L)^2}$$

$$Q_{pq}^{XE} = \frac{\eta}{R_s} \frac{\omega_{pq}^{XE}}{c} \left( \frac{4}{L(1 + \delta_{0q})} + \frac{1}{(\chi_p^{XE})^2} \int_{C_s} |\nabla \psi_p^{XE}|^2 dC_s \right)^{-1}$$

$$E_{pq}^{XE} = \sqrt{\frac{2 - \delta_{0q}}{L}} \frac{\chi_p^{XE}}{\sqrt{(\chi_p^{XE})^2 + (q\pi/L)^2}} \psi_p^{XE} \cos \frac{q\pi z}{L}$$

$$H_{pq}^{XE} = \sqrt{\frac{2 - \delta_{0q}}{L}} \frac{1}{\chi_p^{XE}} \nabla \psi_p^{XE} \cos \frac{q\pi z}{L}$$

$$\int_S (\psi_p^{XE})^2 dS = 1 \quad (\text{normalization})$$

$$h_{mn}^{TE} = \sqrt{\frac{L(2 - \delta_{0m})(2 - \delta_{0n})}{a[L^2 + (na/m)^2]}} \sin \frac{m\pi \xi}{a} \cos \frac{n\pi z}{L}$$

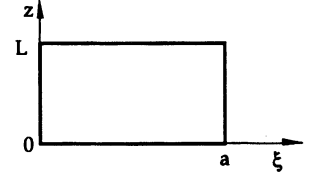
$$h_{mn}^{TM} = \sqrt{\frac{a(2 - \delta_{0m})(2 - \delta_{0n})}{L[(mL/n)^2 + a^2]}} \sin \frac{m\pi \xi}{a} \cos \frac{n\pi z}{L}$$


TABLE 1 Expressions of the resonant frequencies,  $Q$ -factors and modal fields in the case of a cylindrical cavity, as function of eigenfunctions  $\psi$ 's and eigenvalues  $\chi$ 's defined in Section 2. The compact labelling (subscript  $i$ ) is replaced by the extended labelling used in Section 2 ( $X$  represents  $S$  or  $A$ ). The table gives also the functions  $h_{mn}^{TE}$  and  $h_{mn}^{TM}$ , i.e. the transverse-to- $z$  component of the magnetic mode vectors for the  $TE$  and  $TM$  modes in a rectangular waveguide.

an 'equivalent pillbox,' i.e., a pillbox cavity with the same height  $L$  as our structure and with its fundamental mode at the frequency of our  $TM_{10}^{SE}$  mode. In the same way,  $Re\{Z_{\perp}\}$  is normalized to the transverse impedance  $R_{\perp}$  of the first deflecting mode of the same pillbox. The values of the reference resistances can be determined analytically and are given in the figure captions. Figs. 8a and 9a were obtained assuming matched terminations for all the modes, i.e., admittances  $Y_p$  in Eq. (13) were identified with the characteristic admittance of the corresponding waveguide mode. For comparison, Figs. 8b and 9b show  $Re\{Z_{\parallel}\}$  and  $Re\{Z_{\perp}\}$  for the shorted structure ( $Y_p \rightarrow \infty$ ). As anticipated by the qualitative considerations of Section 2, the only peaks surviving in the loaded structure are those in the plot of  $Re\{Z_{\parallel}\}$ . They correspond to the fundamental  $TM_{10}^{SE}$  mode and to the higher-order  $TM_{1q}^{SE}$  modes trapped together with it. Apart from these peaks, the frequency behavior of both impedances is flat, which confirms the suppression of all HOMs other than the  $TM_{1q}^{SE}$  modes. Furthermore, the shunt impedance at the accelerating frequency is only about 20% below the value of the shunt impedance of the pillbox. Apart from the surviving peaks, the wideband impedances are typically between  $-30$  and  $-40$  dB. The number of peaks in Figs. 8b and 9b helps one appreciate the number of resonant modes occurring up to 15 GHz in the shorted structure. The total number of resonant modes used in the calculation was indeed much higher, because all

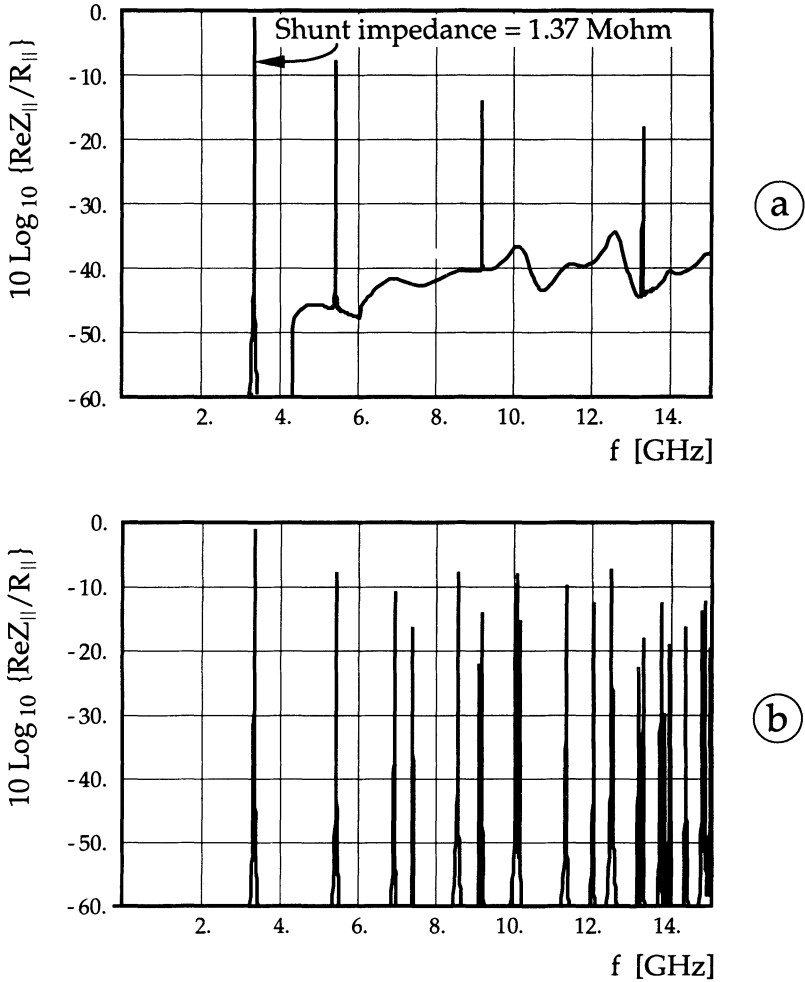


FIGURE 8 Real part of the longitudinal impedance, numerically evaluated for the cylindrical structure of Fig. 2, in the case  $r = 30 \text{ mm}$ ,  $a = L = 35 \text{ mm}$ ,  $d = 73 \text{ mm}$ . The impedance is normalized to  $R_{||} = 1.745 \text{ M}\Omega$ , i.e., the shunt impedance of the ‘equivalent pillbox.’ a) Matched loads connected to the ports. b) Shorted ports.

the resonances up to 20 GHz were considered (58  $\text{TM}^{\text{SE}}$  modes and 90  $\text{TM}^{\text{AE}}$  modes deriving from 16  $\psi^{\text{SE}}$  and from 26  $\psi^{\text{AE}}$  eigenfunctions, respectively). The number  $P$  of waveguide modes considered in the calculations was 22, corresponding to the modes which can propagate below 16 GHz.

A second experiment was performed in order to investigate the effect of a mismatch in the absorbing terminations. In this case the loads were simulated by waveguides

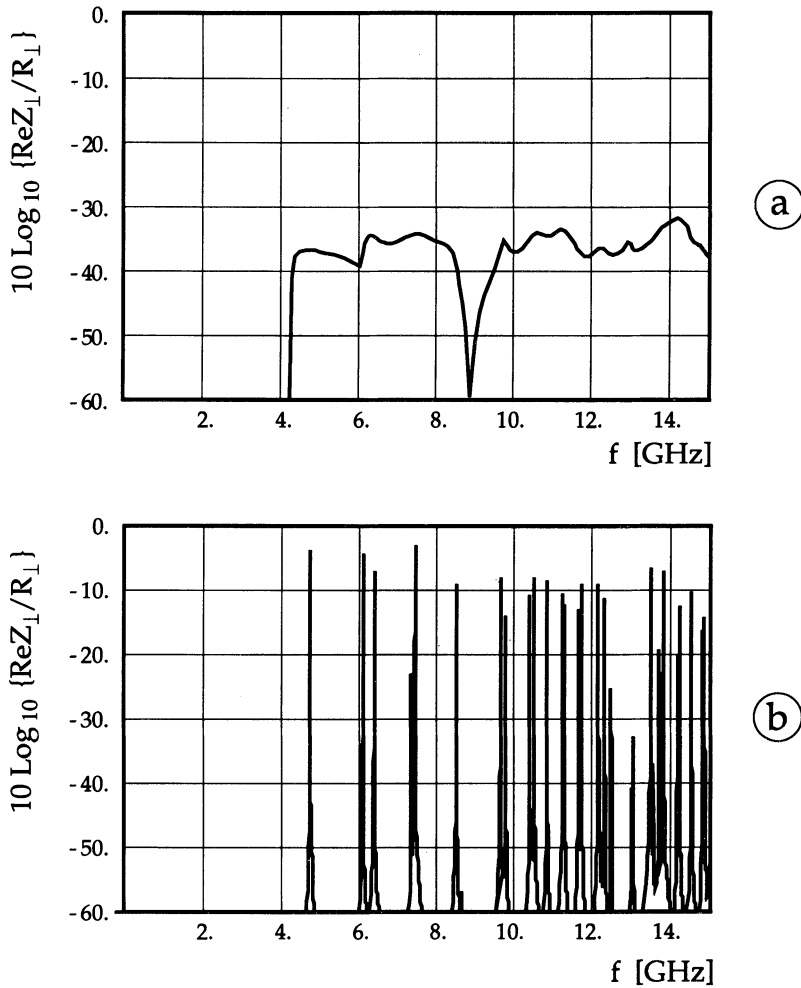


FIGURE 9 Real part of the transverse impedance, numerically evaluated for the cylindrical structure of Fig. 2, in the case  $r = 30 \text{ mm}$ ,  $a = L = 35 \text{ mm}$ ,  $d = 73 \text{ mm}$ . The impedance is normalized to  $R_{\perp} = 47.5 \text{ K}\Omega/\text{mm}$ , i.e., the transverse impedance of the first deflecting mode in the 'equivalent pillbox.' a) Matched loads connected to the ports. b) Shorted ports.

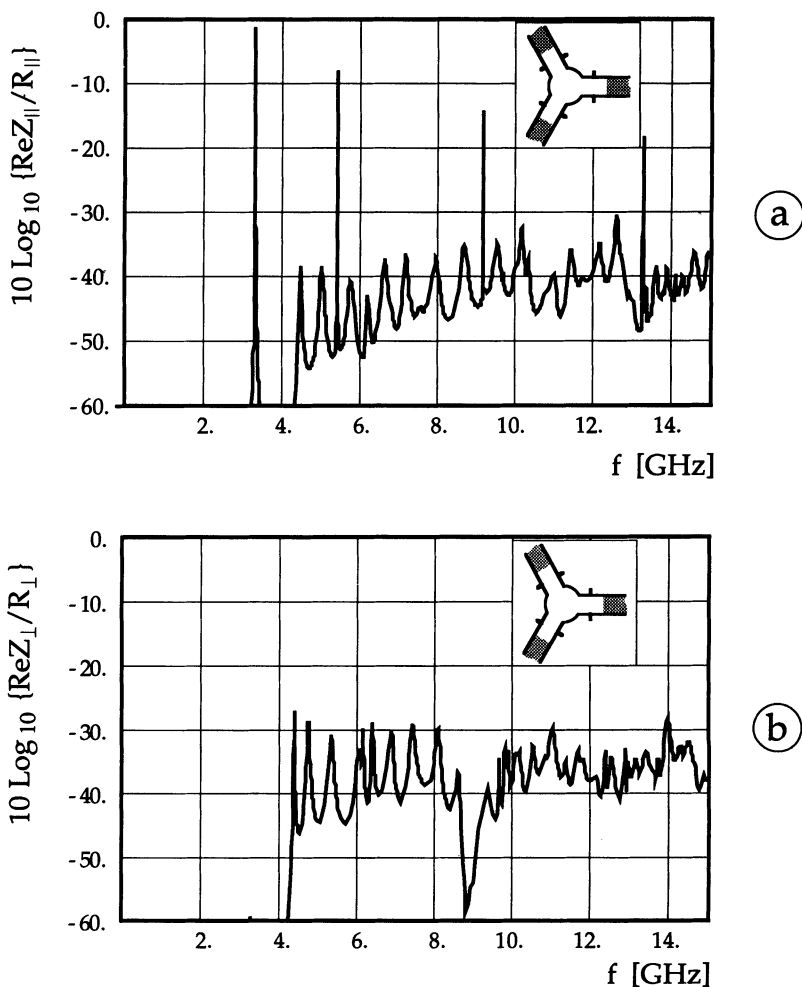


FIGURE 10 Effect of a mismatch of the loads connected to the waveguides: a poorly matched termination is simulated considering a lossy dielectric filling the waveguides. The dielectric characteristics are  $\epsilon_r = 9$  and  $\tan \delta = 0.1$  at 3 GHz ( $\tan \delta$  increases linearly with frequency in the simulation) and the dielectric interface is placed 70 mm from the ports. a) Real part of the longitudinal impedance. b) Real part of the transverse impedance.

filled with a lossy dielectric, beginning at 70 mm from the ports (see the inset in Fig. 10). With the value of permittivity given in the figure caption, the typical VSWR of these terminations is rather high – on the order of 3 for all the propagating modes. The resulting impedances are plotted in Figs. 10a and 10b which show that the mismatch gives rise to a ripple, presumably harmless in most cases.

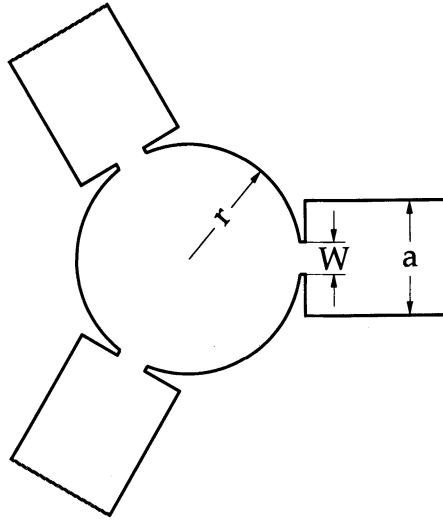


FIGURE 11 Cross section of the cylindrical structure used in the simulations summarized in Fig. 12. The circular central body is connected to the waveguides through longitudinal slots of width  $W$ .

In the structure considered so far the impairment of the shunt impedance of the accelerating mode with respect to the pillbox depends on two factors: a) the lowering of the  $Q$  of the accelerating mode due to the nonuniformities of the wall currents, and b) the decrease of  $R/Q$  due to the spread of the mode field into the lateral waveguides. Though the 20% decrease in the shunt impedance reported before seems to be acceptable in most cases, an investigation was conducted to determine whether reducing the coupling between the central body and the waveguide could increase the shunt impedance without affecting the HOM suppression significantly. We considered inductive irises of width  $W$  at the junction between the central body and the waveguides (see Fig. 11). Many experiments<sup>11</sup> were carried out with values of  $W/a$  ranging from 0.2 to 1 (the latter corresponding to no iris). In these experiments the ratio  $a/r$  was 1. The results are summarized in Fig. 12, which reports the shunt impedance (normalized to  $R_{||}$ ) versus  $W/a$ , together with the minimum monopole HOM damping. (For any HOM, the damping is intended as the difference, in dB, between the peak value of  $Re\{Z_{||}\}$  with and without absorbers). All HOMs in a frequency band up to five times the fundamental are considered, apart from trapped  $TM_{1q}^{SE}$  modes. If we assume that a 30-dB damping of the HOMs' resonant peaks is acceptable, an iris width  $W = 0.5a$  can be used, with the advantage of limiting the shunt impedance reduction to only 7% with respect to the pillbox. Note also that reducing the width to  $W = 0.2a$ , i.e., a coupling comparable to that of conventional HOM dampers, results in very poor HOM damping – below 10 dB. This confirms the importance of accurate coupling-region design.

The last numerical experiment concerned the damping of the residual higher order trapped modes by offsetting the lateral waveguides, as discussed in Section 2 and shown in Fig. 5b. The structure with the offset is no longer cylindrical, and the numerical evaluation of the three-dimensional eigenvectors is now much more laborious. For this reason the impedance calculation was limited to a frequency band much smaller than



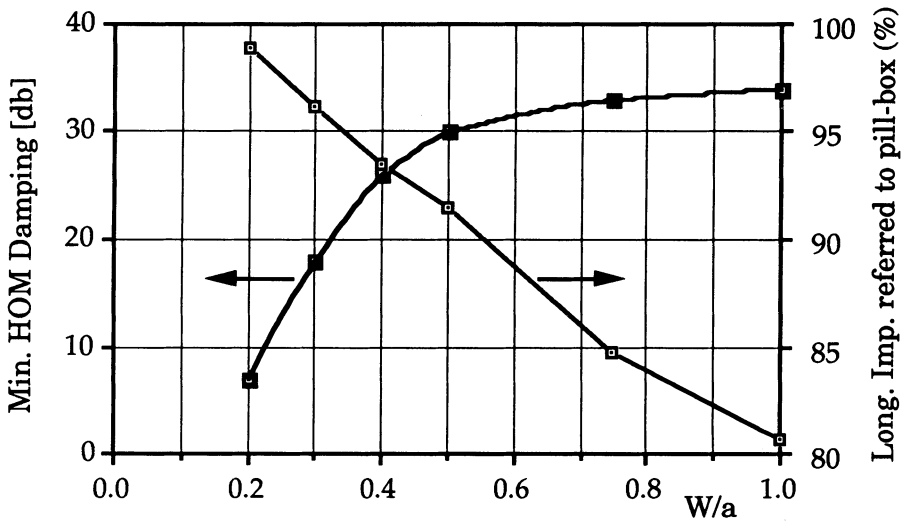


FIGURE 12 Minimum monopole HOM damping (left scale) and reduction of the shunt impedance of the accelerating mode (right scale) for the structure of Fig. 11, in the case  $a/r = 1$ , and for varying  $W/a$ . For any HOM, the damping is intended as the difference in  $db$  between the peak value of  $Re\{Z_{||}\}$  with and without absorbers (trapped  $TM_{1q}^{SE}$  modes are not considered). The reduction of the shunt impedance is referred to  $R_{||}$ . ('equivalent pillbox').

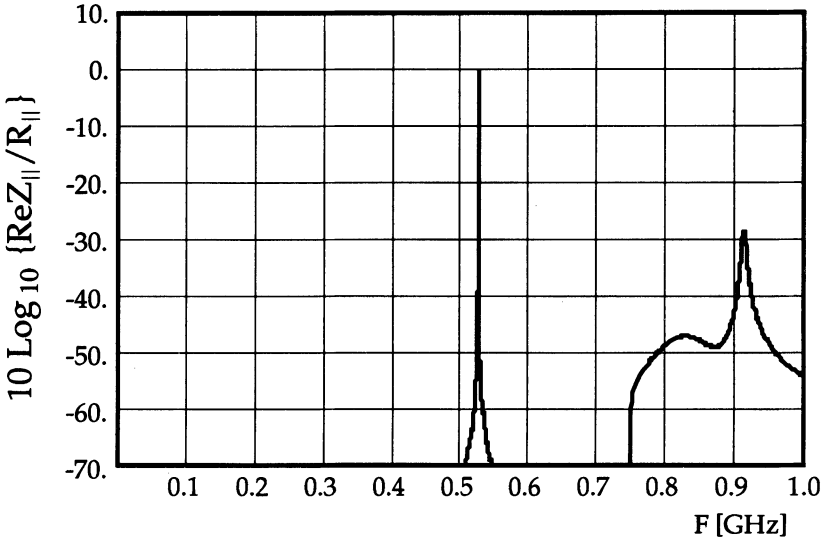


FIGURE 13 Real part of the longitudinal impedance of a quasi-cylindrical STMR operating at 500 MHz, in the case of offset waveguides (Fig. 5b). The dimensions are:  $r = a = L = 200$  mm, and  $\delta = 30$  mm.

before, up to a frequency that would permit investigation of the damping of the first higher-order trapped mode. The experiment was performed<sup>11</sup> referring directly to a full-scale structure operating at an accelerating frequency of about 500 MHz. The dimensions of the structure were  $r = a = L = 200$  mm, and an offset of 30 mm was considered. The calculation of the eigenvectors was performed using a standard three-dimensional electromagnetic solver (ARGUS). The resonant frequencies of the modes corresponding to the  $TM_{10}^{SE}$  and  $TM_{11}^{SE}$  modes in the structure without the offset were 527 and 919 MHz, respectively. Figure 13 shows a plot of  $Re\{Z_{||}\}/R_{||}$  in the 0 - 1 GHz band; note that the peak around 919 MHz is about 30 dB below the value at the accelerating frequency, a result that compares well with the experimental results reported in Fig. 6c.

## 8. CONCLUSIONS

The experimental tests and the numerical simulations reported above have shown that HOM-free accelerating structures are feasible. The basic concept underlying their design consists in imbedding some absorbers in the structure, and in shaping it in such a way as to confine a single high- $Q$  resonating mode far away from them. This mode is strong enough in the interaction region to be used for acceleration. The decoupling between the accelerating mode and the absorbers is achieved using waveguide sections, which operate slightly below cutoff at the accelerating frequency and are connected to the interaction region through large apertures. In contrast to conventional HOM dampers, the loaded waveguides are integrated as a part of the structure from the very beginning of the design rather than being added as a cure. This permits optimized results. Though the shunt impedance of the accelerating mode is slightly lower than that of a conventional cavity, its impairment seems to be an acceptable price in applications where stability requirements are very stringent. In any case, it was shown that this impairment can be minimized by

careful design of the coupling region between the central body and the loads. The use of Computer-Aided Design tools is mandatory for obtaining optimized results. For this reason an algorithm has been presented which permits calculation of the longitudinal and transverse beam-coupling impedances. When considering three-dimensional structures the computing time becomes very long due to the need of calculating many resonant modes of the structure with good accuracy. The availability of three-dimensional solvers more efficient than those available at present could make the described method easier to use in the design of three-dimensional STMRs.

## ACKNOWLEDGMENTS

The authors wish to thank S. Chattopadhyay and G. Lambertson from Lawrence Berkeley Laboratory and M. Puglisi from Sincrotrone Trieste for the stimulating discussions; M. Allen, A. Hutton and H. Schwarz from the Stanford Linear Accelerator Center for their interest in this work and their encouragement; and K. Ko and R. Pendleton from SLAC for providing the results of the ARGUS test example.

## REFERENCES

1. A. Hofmann, 'Single beam collective phenomena - longitudinal,' lecture note in *Theoretical Aspects of the Behaviour of Beams in Accelerators and Storage Rings*, CERN report 77-13, pp. 139-174.
2. D. M. Dykes and B. Taylor, 'Further development of the SRS rf system', in *Proceedings of the IEEE Particle Accelerator Conference* (Washington, D.C., 1987).
3. A. F. Jacob, G. R. Lambertson, and W. Barry, 'Higher order mode damping in an ALS test cavity,' in *Proceedings of the Second European Particle Accelerator Conference* (Nice, France, 1990), pp. 928, 930.
4. Y. Yamazaki, K. Takata, and S. Takumoto, 'Damping test of higher-order modes of the re-entrant accelerating cavity,' *IEEE Trans. Nucl. Sci.* NS-28, 3 (June 1981), pp. 2915, 2917.
5. A. Massarotti, G. D'Auria, A. Fabris, C. Pasotti, C. Rossi, and M. Svandrlík, '500 MHz cavities for the Trieste synchrotron light source ELETTRA,' in *Proceedings of the Second European Particle Accelerator Conference* (Nice, France, 1990), pp. 919, 921.
6. H. Deruyter, Z. D. Farkas, H. A. Hoag, K. Ko, N. Kroll, G. A. Loew, R. H. Miller, R. B. Palmer, J. M. Paterson, and J. W. Wang, 'Damped accelerator structures,' in *Proceedings of the Second European Particle Accelerator Conference* (Nice, France, 1990), pp. 520, 522.
7. G. Conciauro and P. Arcioni, 'A new HOM-Free accelerating resonator,' in *Proceedings of the Second European Particle Accelerator Conference* (Nice, France, 1990), pp. 149-151.
8. G. Dôme, 'RF systems: waveguides and cavities,' lecture given at the Fifth US Summer School on High Energy Particle Accelerators (Stanford Linear Accelerator Center, July 1985), CERN report SPS/86-24.
9. J. Van Bladel, *Electromagnetic Fields* (Hemisphere Publishing Company, 1985), chapter 10.
10. M. Abramowitz and I. A. Stegun, *Handbook of Mathematical Functions* (Dover Publications, Inc., New York, 1965).
11. P. Arcioni, 'POPBCI - a post-processor for calculating beam coupling impedances in heavily damped accelerating cavities,' Stanford Linear Accelerator Center report SLAC-PUB-5444 (1991).
12. P. Arcioni, M. Bressan, and G. Conciauro: 'PAGODA: a computer code for the analysis of waveguides,' Dipartimento di Elettronica dell'Università di Pavia, RI 03/90.